ELSEVIER

Polymer 42 (2001) 9975–9985

polymer

www.elsevier.com/locate/polymer

# Temperature dependence of polymer crystalline morphology in nylon 6/montmorillonite nanocomposites

Derek M. Lincoln[a], Richard A. Vaia[a,*], Zhi-Gang Wang[b], Benjamin S. Hsiao[b], Ramanan Krishnamoorti[c]

[a]*Air Force Research Laboratory, Materials and Manufacturing Directorate Wright-Patterson AFB, OH 45433-7750, USA*
[b]*Department of Chemistry, State University of New York at Stony Brook, Stony Brook, NY, 11794-3400, USA*
[c]*Department of Chemical Engineering, University of Houston, Houston, TX 77004-4792, USA*

Received 2 April 2001; accepted 19 July 2001

**Abstract**

The influence of nanodispersed montmorillonite layers and process history on the crystal structure of nylon 6 between room temperature and melting is examined with simultaneous small- and wide-angle X-ray scattering and modulated differential scanning calorimetry. For the examined process history, nylon 6 exhibits predominantly α-phase behavior from room temperature to melting, with a gradual shift in chain–chain and sheet–sheet spacings from ~100°C to melting. In contrast, the presence of aluminosilicate layers stabilizes a dominant γ-crystal phase, which persists, essentially unmodified, until melting. The temperature dependence of the total crystallinity and the relative fractions of α- and γ-phases is strongly dependent on the layered silicate content and the interaction between the nylon 6 and the aluminosilicate layers. Additionally, the temperature dependence of the α- and γ-phases imply that the γ-phase is preferentially in the proximity of the silicate layers, whereas the α-phase exists away from the polymer–silicate interphase region: In general, process history and use-temperature will determine the relative fraction of the crystalline polymer phases in semi-crystalline polymer nanocomposites, and thus have significant influence on the stability of the crystalline region at elevated temperatures. © 2001 Published by Elsevier Science Ltd.

*Keywords*: Nylon 6; Nanocomposites; Wide-angle X-ray scattering

## 1. Introduction

The explosion of polymer-layered silicate nanocomposites (PLSN) research over the last decade has a great deal to do with their demonstrated enhancements, relative to the neat resin of a suite of physical properties [1–10]. PLSN typically exhibit increased modulus [1,2], impact strength [1,3], heat distortion temperature (HDT) [1,2] and barrier properties [4–6] with decreased thermal expansivity [7]. PLSN are also finding new applications due to their reduced flammability [8], resistance to UV degradation [9], resistance to atomic oxygen [10] and improved ablative performance [11]. In contrast to traditional micron sized fillers such as talc, carbon black, silica or mica, which nominally require loadings of 20 wt% or more, PLSN achieve these enhanced properties with as little as 5 wt% addition of a dispersion of 1 nm thick aluminosilicate layers with diameters between 20 (laponite) and 500 nm (representative montmorillonite) [14]. This low volume addition of reinforcing phase allows the resins to be processed using traditional techniques as well as maintain a degree of optical clarity. Recent review articles give a summary of the structure of layered silicates, approaches to synthesis and property enhancements [12].

Besides property enhancements, PLSN also raise intriguing questions regarding their fundamental behavior, especially in the case of PLSN fabricated from semicrystalline polymers. Initial studies by the Toyota research group suggested the coexistence of the γ and the more-stable α polymer crystalline phases in the nylon 6 based nanocomposites [1]. Further, other studies have found that the γ-crystalline phase of nylon 6 tends to be more ductile than the α-phase [13], which may help to explain the toughness of nylon 6 nanocomposites. Other studies have also found that the presence of the layered silicate disrupts crystalline formation and in certain cases leads to a secondary structure arising from long range (>20 nm) ordering of the layered silicates [14].

Semicrystalline PLSN, such as nylon 6 nanocomposites, are a three (not two) phase, nanoscale system, comprised of

* Corresponding author. Tel.: +1-937-255-9184; fax: +1-937-255-9157.
*E-mail address:* richard.vaia@afrl.af.mil (R.A. Vaia).

0032-3861/01/$ - see front matter © 2001 Published by Elsevier Science Ltd.
PII: S0032-3861(01)00542-0

layered silicate, amorphous polymer regions and crystalline polymer regions. Thus, studies to ascertain the role of the relatively rigid nanoscale filler in improvements of mechanical properties must consider more than stress transfer in a two-phase system. They must also consider how the nanoscale filler alters the development, connectivity and relative concentration of amorphous and crystalline polymer regions, since these factors dictate the mechanical response of a pure semicrystalline polymer. Adequate comparison of experimental results between studies necessitates careful characterization of the semicrystalline polymer morphology, and thus an understanding of the temperature dependence and influence of process and elevated temperature use history on polymer crystallite fraction and distribution.

The objective of this study is to examine the general behavior of the polymer crystalline regions in nylon 6/layered silicate nanocomposites. Several experimental techniques are used to provide an understanding of the behavior of these materials on a global, crystalline region and crystal lamella scale. Simultaneous small-angle (crystal lamellae) and wide-angle (crystalline regions) X-ray scattering methods along with modulated differential scanning calorimetry (MDSC) are employed to provide detailed information on: (1) the sensitivity of the polymer crystallite structure to processing history and (2) the influence of the amount of dispersed layered silicate and polymer-layered silicate interaction on the temperature dependence of the structure of the crystalline regions of nylon 6. Understanding polymer recrystallization, morphology and phase structure at elevated temperatures yields insights to the elevated temperature behavior of semicrystalline polymer nanocomposites.

## 2. Experimental

### 2.1. Materials

Commercially available 2 (NCH2) and 5 (NCH5) wt% layered silicate/nylon 6 in-situ polymerized PLSN materials and pure nylon 6 polymer (Nyl6) were obtained from Ube Industries, Ltd (Japan) [15]. Ring-opening polymerization of ϵ-caprolactam initiated by the pendant carboxylic acids on the surface of the modified montmorillonite reportedly results in approximately 50% (NCH5) and 30% (NCH2) of the nylon 6 chains 'tethered' to the surface of the montmorillonite via ionic interaction of the primary ammonium cation [15]. The resultant weight average molecular weights of the nylon-6 polymer in PLSN are 22,200 (NCH2) and 19,700 (NCH5) g/mol, respectively [16]. A melt-processed nylon 6 PLSN obtained from Southern Clay Products (Gonzalez, TX) was also examined [17]. In contrast to the in-situ polymerized material, weak secondary interactions such as Lewis acid/base and dispersive interactions, dominate the polymer–silicate interactions in the melt processed NLS4 resulting in drastically different polymer–silicate nanoscopic and interfacial morphologies.

The PLSNs were obtained as extruded pellets and dried under vacuum at 70–80°C for 3–4 h prior to compression molding into 7 mm (X-ray scattering) and 25 mm (MDSC) circular disks ~1 mm thick. Platens of a hydraulic press were pre-heated to ~280°C. The mold containing pellets was placed between the platens and heated to ~240°C for several minutes before 500 lbs of pressure was applied. The pressure was kept constant as the mold was heated gradually to ~230–240°C over approximately 12 min. The mold was removed, placed on room-temperature steel heat sink and allowed to cool to room temperature in the ambient. This provided the initial process state for compression-molded samples.

### 2.2. Modulated differential scanning calorimetry

MDSC was carried out using a TA 2920 with a two-point calibration using indium and tin under nitrogen purge. Temperature scans were carried out at 3°C/min from 30 to 250°C on the extruded pellets and compression-molded disks after initial drying in vacuum at 110°C overnight. Percent initial crystallinity was calculated by subtracting the non-reversible heat flow from the reversible heat flow and dividing by the heat of crystallization for nylon 6 (190 J/g) [18].

### 2.3. X-ray characterizaton

Simultaneous small-angle (SAXS) and wide-angle (WAXS) X-ray scattering experiments were conducted at the Advanced Poylmers Beamline (X27C) of the National Synchrotron Light Source (NSLS), Brookhaven National Laboratory (BNL). The wavelength of the incident X-rays was 1.307 Å defined by a double multi-layer monochromator. The synchrotron X-rays were collimated to a 600 μm beam size using a three-pinhole collimator [19]. Data were collected using two linear position sensitive detectors [20] at 190 (SAXS) and 20 (WAXS) cm. The scattering angle was calibrated using silver behenate (SAXS) and quartz (WAXS) powder samples. Samples, mounted in copper holders, were placed in the beam in a small temperature chamber that was heated at a rate of approximately 2°C/min from room temperature to ~250°C. Details of the dual-chamber temperature jump apparatus can be found elsewhere [19]. Data acquisition times were 0.25–4 min per scan. All the X-ray data were corrected for beam fluctuations and sample absorption. Analyses of the small-angle scattering data were carried out as detailed elsewhere [14].

Deconvolution of the superposition of crystalline peaks and broad amorphous halo observed in the WAXS data was carried out using GRAMS/32 Spectral Notebase™ (Galactic Industries Corporation) with Gaussian peak shape. The analyses yielded integrated intensities, peak positions, peak heights and peak widths of the respective crystal

reflections and amorphous background. One Gaussian peak was used to describe the amorphous phase. The apparent degree of crystallinity, $\phi_{mc}$, is proportional to the ratio of the total intensity of crystalline reflections to the total observed intensity (crystalline + amorphous).

### 2.4. Terminology

As a result of the multicomponent nature of semicrystalline PLSN, confusion may arise pertaining to the terminology used to describe the various features. Throughout this text, the following terminology has been adopted: 'silicate crystallite' (or tactoid) refers to the original, unintercalated organically modified aluminosilicate layers, 'silicate layer' refers to the individual montmorillonite (aluminosilicate) sheets, 'lamellar stack' refers to a polymer lamellar superstructure consisting of alternating layers of crystalline and amorphous polymer, 'crystal layer' refers to the crystalline regions of the lamellar stack, and unless further specified 'crystalline' and 'amorphous' refers to all such polymer regions whether incorporated within or external to the polymer lamellar stack.

## 3. Results and discussion

For semicrystalline polymers, processing methods and history define the temporal, mechanical and thermal environment, which in turn determine the mobility, relaxation and extent of chain extension, as well as nucleation, growth and orientation of polymer crystallites. Therefore, process and use history dictate the final morphology and thus ultimate thermomechanical properties of semicrystalline polymers. For semicrystalline PLSNs, the final thermomechanical properties are anticipated to be even more susceptible to process history, for the presence of the organically-modified layered silicate (OLS), its distribution and the degree of polymer–silicate interfacial interactions will compound the development of polymer crystallite morphology and increase the complexity of processing structure–property relationships. Thus, subsequent conclusions herein, as well as elsewhere, relative to the phase behavior and morphology of semicrystalline PLSNs and relation to final PLSN properties, must be understood within context of the specific process history of the material.

To develop an understanding of these relationships, two different types of semicrystalline PLSNs are examined in this study — in-situ polymerized and melt-processed — to ascertain the influence of the polymer–silicate interfacial structure on the subsequent morphological development of the semicrystalline polymer. In-situ polymerization, initiated by the terminus of the organic modification of the OLS, ostensibly creates a stronger polymer–silicate interfacial region, consisting of ionically associated and stretch polymer chains, than achieved via melt processing of polyamide with an OLS with non-reactive organic modifications, whose interfacial region is simplistically envisioned as consisting of secondary interactions between the silicate surface, alkyl chains and polyamide. The exact structure of the interface and its temperature dependence is, to-date, not well characterized though. Nonetheless, for the purpose of this study, these two types of polyamide nanocomposites epitomize the relative differences between strong (NCH2, NCH5) and weak (NLS4) interfacial interactions.

### 3.1. Thermal behavior

Fig. 1(a) and (b) summarizes the total heat flows (MDSC) for the extruded pellets and the compression-molded samples of nylon 6, NCH2, NCH5 and NLS4 after annealing for 12 h at 110°C in vacuum. Temperature profiles for the extrusion and compression molding processes were not monitored in detail and are presented as generally representative of semicrystalline PLSN response to rapid air quench and slow mold cooling, respectively.

Comparison of the traces for the extruded and the compression-molded samples indicate that process history influences the thermal behavior of both pure polymer and nanocomposites. For pure nylon, extrusion and subsequent air cooling results in a broad melting endotherm, and an endothermic peak at the glass transition temperature attributed to a heat capacity overshoots due to physical aging of the amorphous polymer regions. In contrast, compression molding and subsequent heterogeneous cooling experienced by the sample in the mold results in an even broader melting endotherm, an absence of latent heat at the glass transition temperature, and the development of a new endotherm at 125–130°C. Similar processing induced behavior is observed for the nanocomposites.

The presence of aluminosilicate layers causes a slight

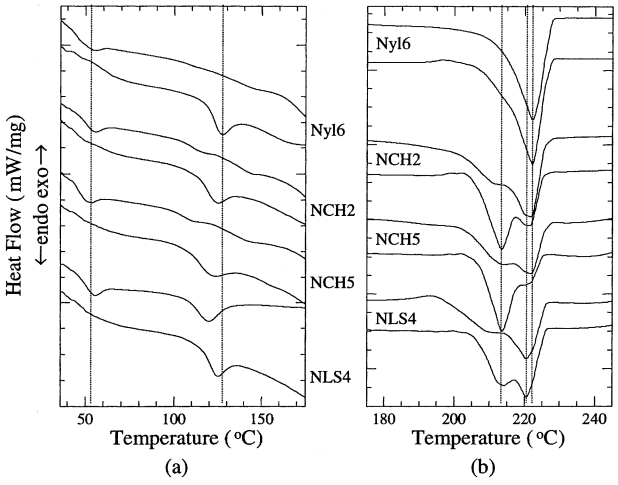


Fig. 1. The total heat flow from heating scans (10°C/min) in modulated DSC (MDSC) for the extruded pellets and the compression-molded samples after both were treated for 12 h at 110°C in vacuum. The top curve in each pair is from the extruded sample and the bottom curve is from the compression-molded sample. Note the magnitude of the abscissa in (a) and (b) is different to enhance detail.

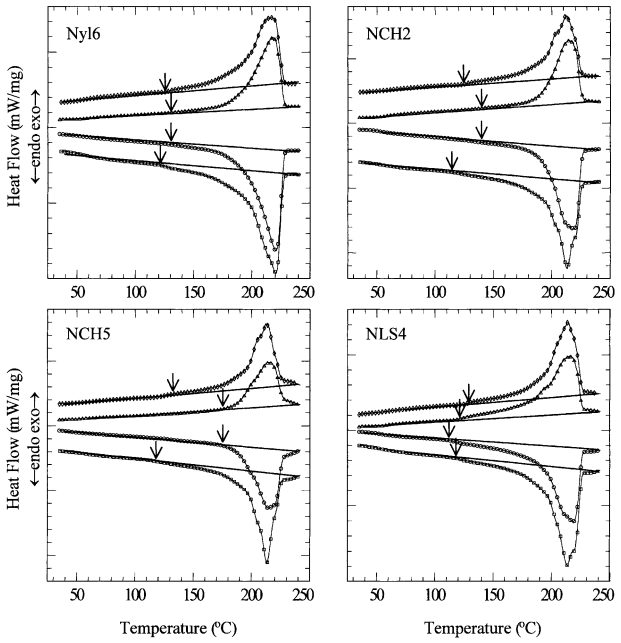


Fig. 2. Reversible and non-reversible heat flow traces from heating scans (10°C/min) in MDSC. The arrows indicate the point at which each of the traces deviates from the baseline. ◇ — compression-molded nonreversible, △ — extruded nonreversible, ○ — extruded reversible, □ — compression-molded reversible.

shift in the main melting peak to slightly lower temperatures (221°C) accompanied by the emergence of a second, lower temperature (213°C) endotherm. The influence of processing on the magnitude of the lower melting endotherm for the strong interface nanocomposites is dramatic — increasing significantly in the case of compression molded NCH2 and NCH5 as compared to their respective extruded samples. On the other hand, for the case of NLS4, only slight differences are observed between the compression molded and extruded nanocomposites.

In general, the breadth and structure of the melting endotherm reflects the type of crystalline phases present as well as the distribution of crystallite size, which depends on crystallization conditions, growth and recrystallization of crystal lamellae and the fraction of low molecular weight chains [21].[1] The lower temperature endotherm has been attributed, in previous studies, to an increased fraction of γ-phase crystallites present in the sample [3]. Following, it is tempting to conclude from Fig. 1 that strong interfacial interactions (NCH2 and NCH5) further promote the formation of the γ-phase upon processing at elevated temperature. However, an alternative hypothesis is that the presence of the silicate promotes the formation of smaller, more disordered crystallites, with lower melting temperature, due to hindered chain motion. X-ray studies presented below favors the later explanation for the melting peak at 213°C.

Competing processes of melting, recrystallization and coarsening of the crystallites between $T_g$ and $T_m$ complicates detailed interpretation of the thermal transitions observed in the total heat flow DSC data shown in Fig. 1. MDSC enables the observation of these overlapping reversible (glass transition) and non-reversible (enthalpic relaxation, crystallization, evaporation, decomposition, and cure) events [22][2]. Fig. 2 shows the reversible and non-reversible heat flow traces for the extruded and compression-molded samples. In contrast to a flat baseline between $T_g$ and melting and the two discrete melting events observed from Fig. 1, reversible and non-reversible heat flows indicate a dynamic environment of crystal formation and melting occurring continuously between ~125 and 230°C in pure nylon and the nanocomposities. For NCH2 and NCH5, compression molding lowers the onset of these phenomena (indicated respectively in the nonreversible and reversible traces [22][2]) relative to extrusion. In contrast, these processes occur at roughly the same temperature for Nyl6 and NLS4, irrespective of the process history examined. Again, it is tempting to conclude that the lack of systematic differences between compression-molded and extruded NLS4 data would suggest (as in the case of the pure nylon 6) that the absence of strong interfacial interactions between the polymer and silicate layers does not result in a significant difference in the crystallization behavior. The layers act merely as Brownian particles and in the absence of 'active communication' between them and the polymer, the polymer, upon crystallization, has the potential to move the silicate layers, so they provide the least disturbance to the crystallization process.

The endothermic peak at ~125°C in the total heat flow trace arises from a difference in the onset temperature of melting of small crystallites (endothermic reversible trace) relative to cold crystallization (exothermic non-reversible trace). Since this behavior is independent of the presence of layered silicate, it probably arises from the heterogeneous nature of compression-molded samples (thermal transfer from sample to mold results in different crystallization histories for the surface and interior of the sample). Note though, the reversible and nonreversible traces in the nanocomposites especially NCH5, do not rapidly return to the baseline after the melting peak, as in pure nylon, but gradually extended up to 240°C. This parallels previous reports of the presence of a small fraction of a high-temperature polymer crystal phase that has been associated

[1] Note that with regards to aging studies of nylon 6, the cumulative effect of polymer degradation during elevated temperature processing increases the fraction of lower molecular weight chains and thus will have a cumulative impact on the crystallization and melting behavior. The role of the layered silicate in polymer degradation during processing has not been examined and, therefore, this factor can not be completely discounted when considering the relative changes in melting behavior before and after compression molding.

[2] Note that melting can occur in both reversible and non-reversible heat flow and strongly depends upon the experimental conditions under which the MDSC is conducted.

Table 1
Percent initial crystallinity from MDSC

| | Processing | Reversible (J/g) | Non-reversible (J/g) | Δ (J/g) | Crystallinity (%)[a] |
|---|---|---|---|---|---|
| Nyl6 | Extruded | 292.8 | 218.2 | 74.6 | 39.3 |
| | Compression-molded | 319.5 | 249.2 | 70.3 | 37.0 |
| NCH2 | Extruded | 269.8 | 199.1 | 70.7 | 37.2 |
| | Compression-molded | 285.8 | 221.4 | 64.4 | 33.9 |
| NCH5 | Extruded | 208.8 | 156.7 | 52.1 | 27.4 |
| | Compression-molded | 289.8 | 247.6 | 42.2 | 22.2 |
| NLS4 | Extruded | 293.2 | 229.1 | 64.1 | 33.7 |
| | Compression-molded | 278.3 | 217.9 | 60.4 | 31.8 |

[a] Initial percent crystallinity based on $\Delta H_{cryst} = 190$ kJ/kg [18].

with the stabilizing presence of the polymer-layered silicate interface [23].

Table 1 summarizes the magnitude of reversible and non-reversible heat flow from MDSC and the calculated percent initial crystallinity for the various samples. With the exception of NLS4, the percent initial crystallinity decreases after compression molding. Also, the percent crystallinity for comparably processed samples generally decreases with increased volume fraction of dispersed layered silicate. Overall, this agrees with previous studies determining crystal content during isothermal crystallization at 205°C [14].

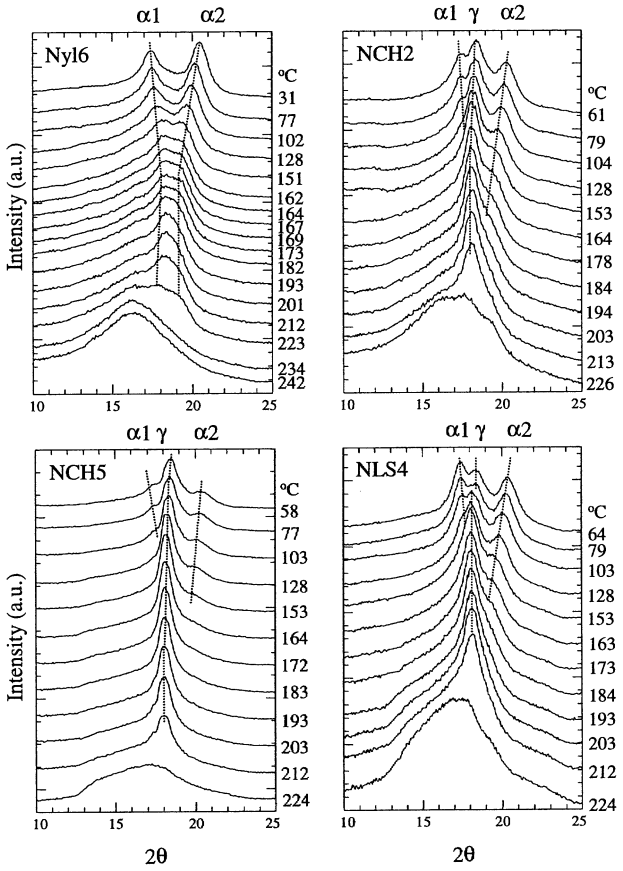


Fig. 3. WAXS profiles at selected temperatures for compression molded nylon 6 and the nanocomposites (NCH2, NCH5, NLS4). The lines approximately represent peak positions. Detailed data from deconvolution are in Fig. 5.

### 3.2. Crystalline structure of nylon 6

For complex systems such as semicrystalline PLSNs, direct in-situ observation of structural changes, such as by X-ray diffraction and scattering, to complement thermal analysis is invaluable. Fig. 3 shows representative wide-angle X-ray scattering (WAXS) data collected at 2°C/min upon heating of pure nylon 6 and NCH2, NCH5 and NLS4 compression-molded nanocomposite samples. Note that specimen geometry for the scattering studies precluded examination of the extruded samples. The assignment of the reflections associated with the α-and γ-crystalline phases of nylon 6 are based on the unit cell and chain configurations reported in the literature [24].[3] An example deconvolution of the WAXS profiles is shown in Fig. 4.

The temperature dependence of the angular location of the reflections, apparent degree of crystallinity and normalized fractions of the different phases are shown in Figs. 5–7,

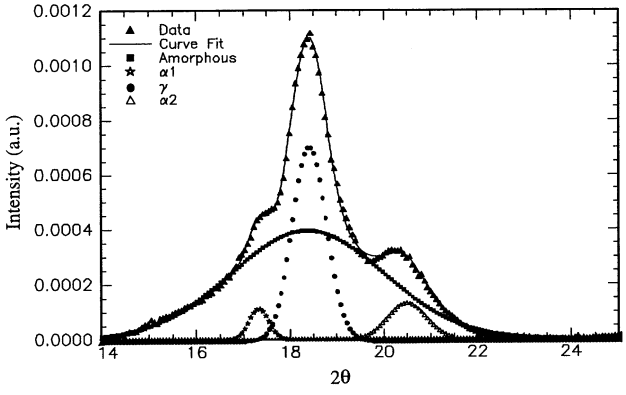


Fig. 4. Representative example of a curve fit of the WAXS data showing the corrected data, overall curve fit, and each of the fitting peaks for NCH5 at 77°C.

[3] Note that conclusive identification of the γ-phase requires observation of the 0 14 0 reflection, which is outside of our experimentally accessible scattering range.

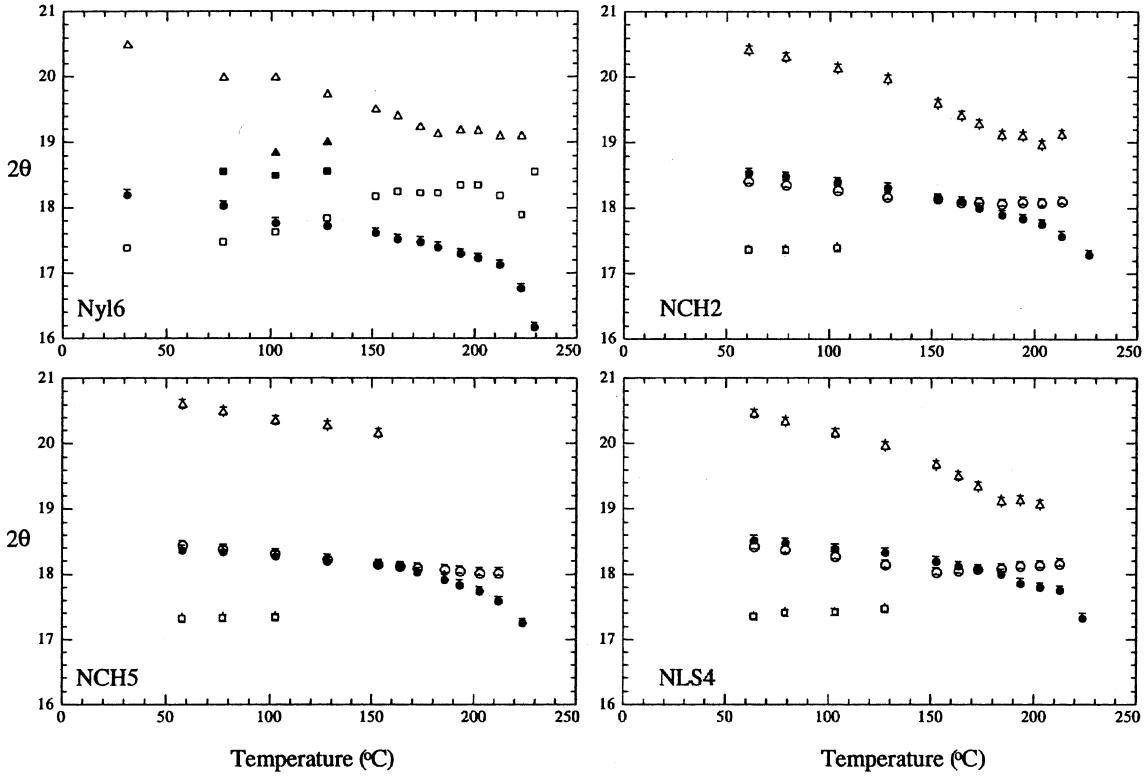


Fig. 5. Position of reflections at various temperatures from deconvolution of the WAXS profiles of compression molded nylon 6 and the nanocomposites (NCH2, NCH5, NLS4). Amorphous — ●, α1 — △, α1′ — ▲, α2′ — ■, α2 — □, γ — ○.

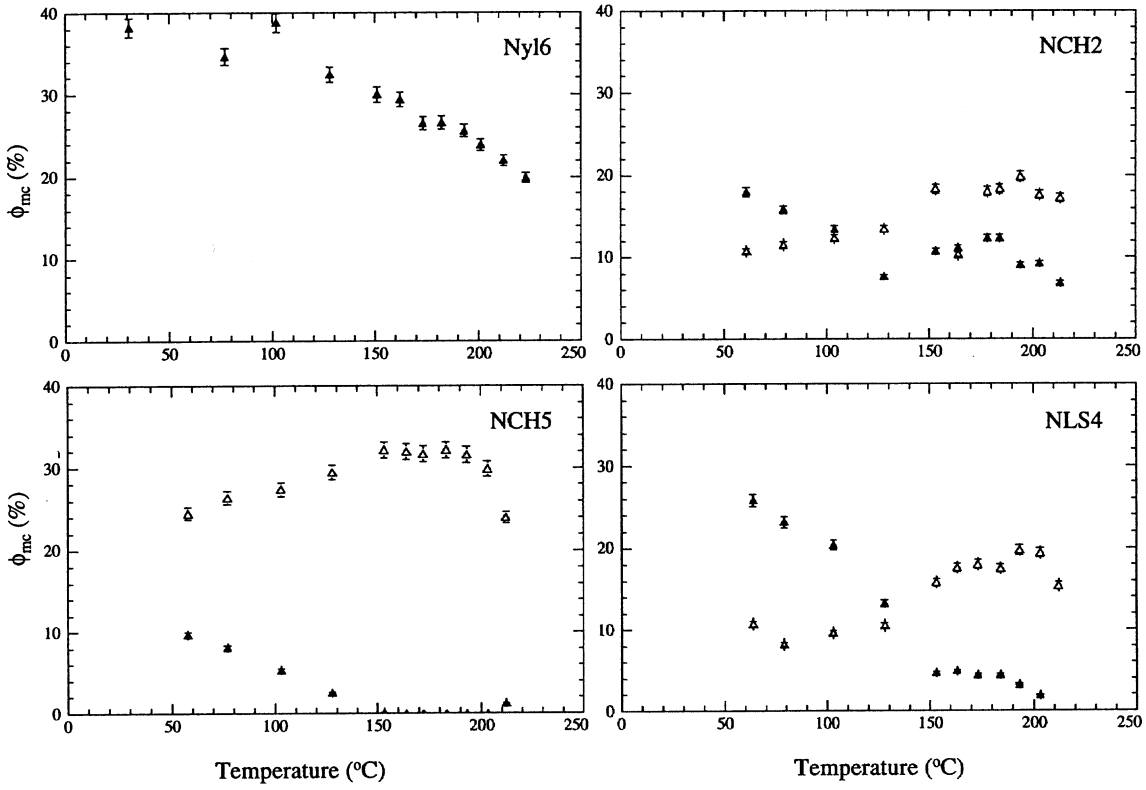


Fig. 6. Apparent degree of crystallinity ($\phi_{mc}$), determine as the ratio of the area of the crystalline reflections to the total area of amorphous and crystalline reflections. α phase — ▲, γ phase — △.

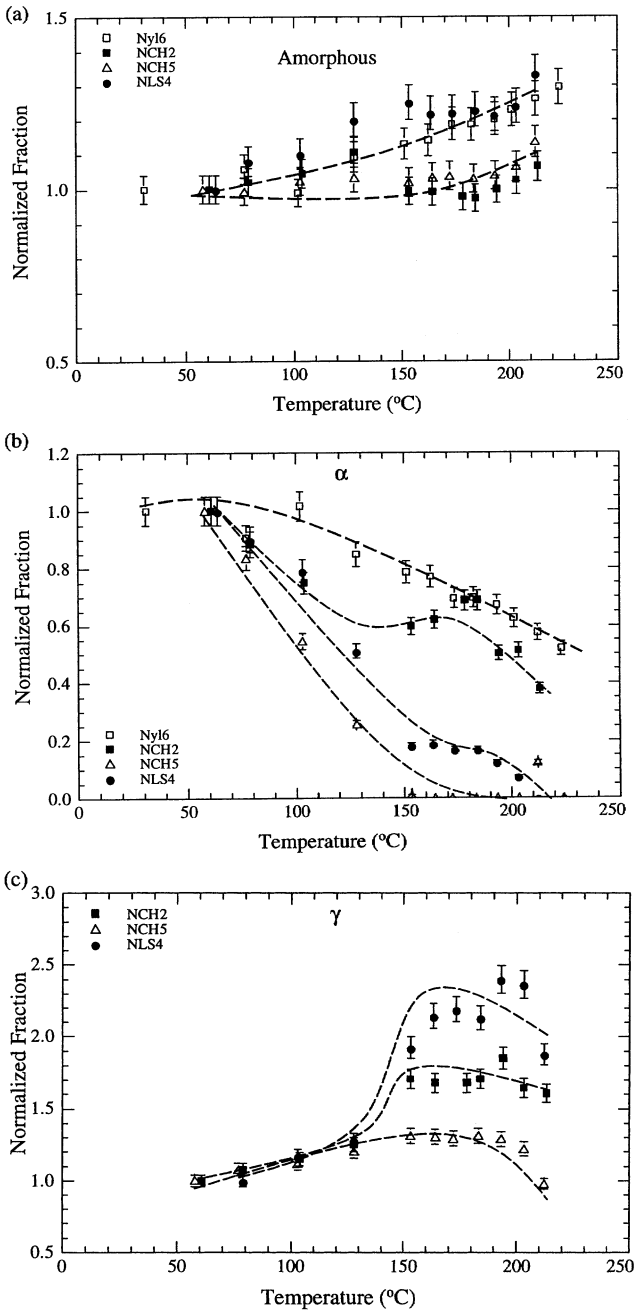


Fig. 7. Comparison of individual phase amounts as a function of temperature. (a) normalized amount amorphous, (b) normalized amount α and (c) normalized amount γ. The amounts are normalized to the amount of each phase present at room temperature. The lines are drawn as a guide to the eye and are not intended to represent a mathematical fit of the data.

respectively. The qualitative processes observed for all the samples upon heating also occur, in reverse, upon cooling (data not shown), with the expected shift to lower temperatures arising from undercooling. This discussion will focus on structural changes upon heating, whereas a following study will discuss the process of isothermal crystallization [25].

For pure nylon 6, the reflections at 17.3 and 20.3 (α1 and α2) indicate that the α-crystalline phase is predominant [24,26].[3] The α-crystalline phase is comprised of an extended, anti-parallel arrangement of chains, which is often attributed to crystallites consisting of folded chains. The absence of a single, sharp peak at the higher temperatures indicates that the distance between hydrogen-bonded chains and the separation of sheets of these hydrogen-bonded chains are maintained and discernible up to the melting temperature. Note that as the chain–chain spacing (higher $2\theta$ reflection) increases with increased temperature (thermal expansion), the sheet–sheet distance (lower $2\theta$ reflection) decreases (thermal contraction) which eventually leads to a pseudo-hexagonal like chain packing. Previous studies of unoriented specimens of nylon 6 have reported the presence of a Brill transition at ~160°C associated with an abrupt change in peak position arising from a transformation between two monoclinic lattices [27,28] or simply due to anisotropic thermal shifts in the unit cell. A similar structural change may also be inferred from the pure nylon results around 180°C, although the transition is not abrupt. The lack of a Brill transition has been previously reported for biaxially oriented nylon 6 specimens [29]. The compression-molded samples used in this study presumably fall between the extremes of unoriented and biaxially oriented samples. Thus, the absence or shift in a Brill transition is not surprising. Optimal deconvolution of the WAXS data required inclusion of two additional reflections, $\alpha 1'$ and $\alpha 2'$, between ~75 and 125°C, which may provide evidence that a small fraction of the crystalline material exhibits a Brill transition, but there is insufficient data to be conclusive. More likely, these additional reflections are associated with a process-history dependent, crystalline phase that is constrained or within very small crystallites, which melts at ~125°C, corresponding with the onset of crystallite melting observed in MDSC. Deconvolution of the WAXS data above 125°C requires only three reflections (amorphous, α1 and α2).

In contrast to pure nylon 6, the nanocomposite scattering curves exhibit a prominent reflection at $2\theta$ ~18.3 at all temperatures. This reflection is indicative of the γ-crystalline phase comprised of a twisted, parallel chain arrangement often attributed to crystallites containing unfolded chains. The single reflection and shift to lower $2\theta$ (and higher spacing) with increased temperature implies that distances between neighboring chains and neighboring sheets are indistinguishable and increase with temperature. The α-crystal phase is also present in NCH2, NCH5 and NLS4, exhibiting the same temperature dependence as observed in pure nylon 6.

The apparent degree of crystallinity ($\phi_{mc}$) with regard to α- and γ-phases (determined as the ratio of the area of the crystalline reflections to the total area of amorphous and crystalline reflections) for each of the samples from room temperature to 205°C is shown in Fig. 6. Consistent with the MDSC studies, the temperature at which the greatest changes in $\phi_{mc}$ of α- and γ-phases begin, roughly

Table 2
Apparent degree of crystallinity ($\phi_{mc}$) for compression molded samples from WAXS ($\phi_{mc}$ = (area of the crystalline reflections)/(area of amorphous and crystalline reflections))

| | Room temperature | | | 205°C | | |
|---|---|---|---|---|---|---|
| | % α | % γ | Total | % α | % γ | Total |
| Nyl6 | 38.1 ± 1.1 | 0 | 38.1 ± 1.1 | 23.9 ± 0.7 | 0 | 23.9 ± 0.7 |
| NCH2 | 17.9 ± 0.5 | 10.7 ± 0.3 | 28.6 ± 0.8 | 9.2 ± 0.3 | 17.6 ± 0.5 | 26.8 ± 0.8 |
| NCH5 | 9.7 ± 0.3 | 24.5 ± 0.7 | 34.2 ± 1.0 | 0 | 29.9 ± 0.9 | 29.9 ± 0.9 |
| NLS4 | 25.8 ± 0.8 | 10.7 ± 0.3 | 36.5 ± 1.1 | 1.9 ± 0.1 | 19.4 ± 0.6 | 21.3 ± 0.7 |

corresponds to the onset of crystalline melting and recrystallization (~125°C) observed in MDSC.

The values of $\phi_{mc}$ for α, γ and total crystallinity at room temperature and 205°C are summarized in Table 2. The magnitude and effect of silicate concentration is different from that inferred from the MDSC measurements. This probably reflects the arbitrary use of a single latent heat of fusion for nylon 6 without specific information on the types and amounts of each phase present and the inherent averaging of crystalline content from room temperature to melting associated with determining crystallinity from DSC.

In Nyl6, the α-crystalline phase is predominant up to melting. Its relative concentration begins to steadily decrease by 38% between 120°C and melting. In contrast, for NCH2 and NLS4 the α-phase is dominant at lower temperatures but is replaced by the γ-phase at higher temperatures (~100 and ~130°C, respectively). For NCH5 the γ-phase is predominant throughout the entire temperature range, with no α-phase present prior to melting. These results contrast conclusions drawn previously from the dual-melting behavior observed in DSC, which assumes both γ- and α-phase is present at melting. In reality, only a minor amount of α is present near melting (much smaller than necessary to account for the relative ratio of the area of the two endotherms in DSC), whereas the γ-phase is present up-to complete melting, as indicated by a discontinuous shift in the scattering curve to lower $2\theta$.

The fraction of γ-phase present at room temperature is higher for NCH2 and NCH5 than NLS4, implying the interfacial interactions between polymer and silicate as well as silicate content influences the amount and type of crystalline phase. Upon heating to 205°C the decrease in the total $\phi_{mc}$ for NLS4 is much greater than for NCH2 and NCH5, suggesting a stabilizing effect of the crystalline regions at elevated temperatures as a result of strong interfacial interactions. Further studies are necessary to determine if this stabilizing effect is of thermodynamic origin (stability of crystalline phase near interfaces) or of kinetic origin (decreased chain mobility associated with silicate–polymer interactions).

Fig. 7 compares the normalized amount of amorphous, α- and γ-phases in each material, emphasizing the temperature dependence of the structural transformations. The relative rate and final extent to which the α-phase decreases with increasing temperature depends on the silicate content. Higher silicate concentration results in an increased rate and extent to which the original α-phase is removed. Correspondingly, the temperature at which the decrease in the α-phase begins is approximately independent of silicate loading or interlayer interactions. The relatively low temperature (50°C) in which the relative amount of α-phase begins to decrease implies that the α-regions in the nanocomposites preferentially consist of the smallest crystallites (lowest melting). As the silicate concentration increases, the volume of polymer removed from silicate interface, where chain-folding crystallization can occur, decreases. In other words, an increased concentration of silicate layers, increasingly disrupting equilibrium crystallite formation.

In contrast to the relative behavior of the α-phase, the rate of formation at elevated temperatures ($T > 140$°C) of additional γ-phase in the nanocomposite depends on both silicate content and interfacial interactions. Decreased chain mobility arising from an increased fraction of strongly interacting polymer chains decreases the extent of elevated temperature growth of γ-phase for NCH5 relative to NCH2. In contrast, the rate of γ-formation is greatest for NLS4. In contrast, increase in the relative amount of amorphous polymer occurs slower and to a less extent in the NCH2 and NCH5 than NLS4 and the pure polymer. This is consistent with the strong polymer–silicate interactions stabilizing the crystalline regions.

On the basis of these observations, it is suggested that the γ-phase forms near the surface of the silicate layers and the α-phase forms removed from the layers, where the influence of the silicate surface on chain conformation and the ability for the chains to fold is not substantial. As the volume fraction of silicate increases, the mean separation between silicate layers drastically decreases [30] and regions where crystallization through chain folding is not hindered by surfaces correspondingly decreases. In conjunction, stronger polymer–silicate interactions effectively increases the width of this interfacial regime, even further inhibiting equilibrium crystallite formation. For NCH2 and NCH5, the extended chain conformation initially dictated by the tethering of the chains to the silicate surface preferentially favors γ-formation. The retardation of the increase in amorphous material until 150°C and the less extensive elevated temperature formation of γ material indicates

that strong polymer–silicate interactions retards chain mobility. For NLS4, the influence of the silicate layers on the crystalline polymer is similar to NCH2 and NCH5 except that the interfacial interactions are weaker and the conformations of near-surface polymer chains are not as drastically disturbed. Here, the layered silicate still hinders chain folding, resulting in the formation of the γ-phase, but chain mobility at elevated temperatures is comparable to pure nylon as demonstrated by the temperature dependence of the amorphous polymer regions.

### 3.3. Lamellar stack morphology of nylon 6 and nylon 6 nanocomposites

Despite the indication of crystalline regions in the nanocomposites via MDSC and WAXS, polymer lamellar stacks are not easily discernable in SAXS. As discussed in previous studies [9], even though the nanocomposites have a comparable amount of crystalline material to pure nylon 6, very little of the crystalline polymer material is incorporated into lamellae structures due to disruption of the lamellae by the presence of the dispersed silicate layers. Detailed analysis of the small angle scattering arising from the polymer mesostructure requires removal of the strong contribution of the silicate layers. As demonstrated previously [14], a point-by-point subtraction of a SAXS pattern collected at $T > T_m$, which only contains scattering from the dispersed silicate, from a pattern collected $T' < T_m$ will yield the net scattering due to the polymer crystal lamella structure at $T'$, assuming the melting or crystallization process does not drastically alter the mean distribution of the silicate. This net SAXS profile can be analyzed using the correlation function method to yield long spacing, crystalline layer thickness and amorphous layer thickness [31]. The viability of directly removing silicate scattering decreases with increasing $\Delta T(\Delta T = T_m - T')$, though. Lack of consistency in the data analysis at the lower temperatures (higher $\Delta T$) indicated that below $T \sim 175$°C, removal of silicate scattering was not complete and correlation function analysis could not be accomplished.

Fig. 8 shows representative SAXS profile at 205°C for nylon 6 and net SAXS profiles at 205°C for the nanocomposites after direct removal of the scattering from the molten nanocomposites (255°C). As is evident from the net SAXS profiles, the layered silicate obscures a small reflection arising from polymer lamellar stacks in the nanocomposites. However, the integrated area of the reflection (proportional to concentration, perfection and size of the lamellar stacks) is substantially reduced in the nanocomposites relative to the pure nylon, even though the $\phi_{mc}$ at 205°C indicates comparable amounts of crystalline material are present.

The partial scattering invariant, $Q^*$, determined from the finite integral of $Iq^2$ with respect to $q$ over the experimental data range $(0.08 < q < 2.5\ \mathrm{nm}^{-1})$, provides a relative measure of the amount and size of the lamellar stacks

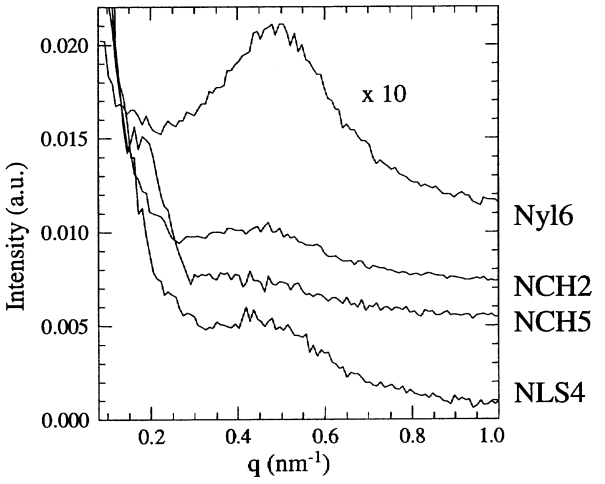


Fig. 8. SAXS profiles at 205°C corrected to remove effects from clay scattering. The profiles are offset for easier viewing.

present in the samples. $Q^*$ for the pure nylon and nanocomposites are shown in Fig. 9 as a function of temperature. It is imperative to recall that the scattering data analyzed using this technique only corresponds to the fraction of crystalline polymer contained within the lamellar stack structures. Thus, from Fig. 9, it can be seen that approximately less than 10% of the crystalline polymer in the nanocomposites are arranged into lamellae. Similarly, the smaller value of $Q^*$ for the nanocomposites implies smaller, more disordered lamellae exist, indicating that the presence of the silicate layers prevents polymer chains from easily being incorporated into the lamellar structure. Note that $Q^*$ increases with temperature in a similar manner as in pure nylon, suggesting that the elevated temperature mechanism of melting of small lamellar stacks and corresponding growth of larger lamellae is generally unaffected by the presence of the silicate.

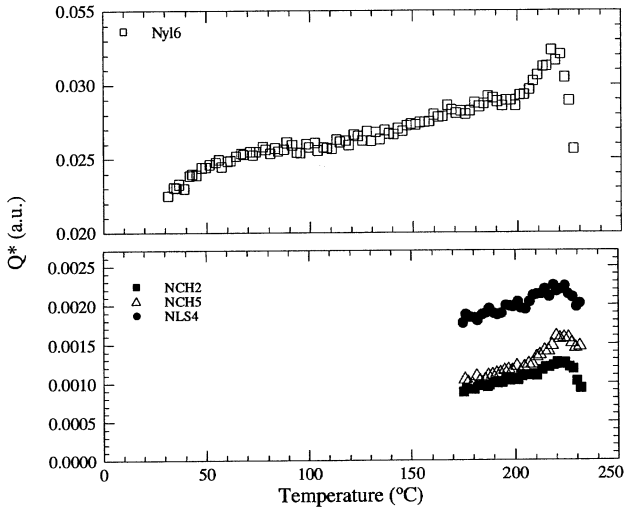


Fig. 9. The partial scattering invariant, $Q^*$, calculated over the experimental $q$ range 0.08–2.5 $\mathrm{nm}^{-1}$ for each sample as a function of temperature. Note the differences in the $y$-axis scales between the upper and lower plots.

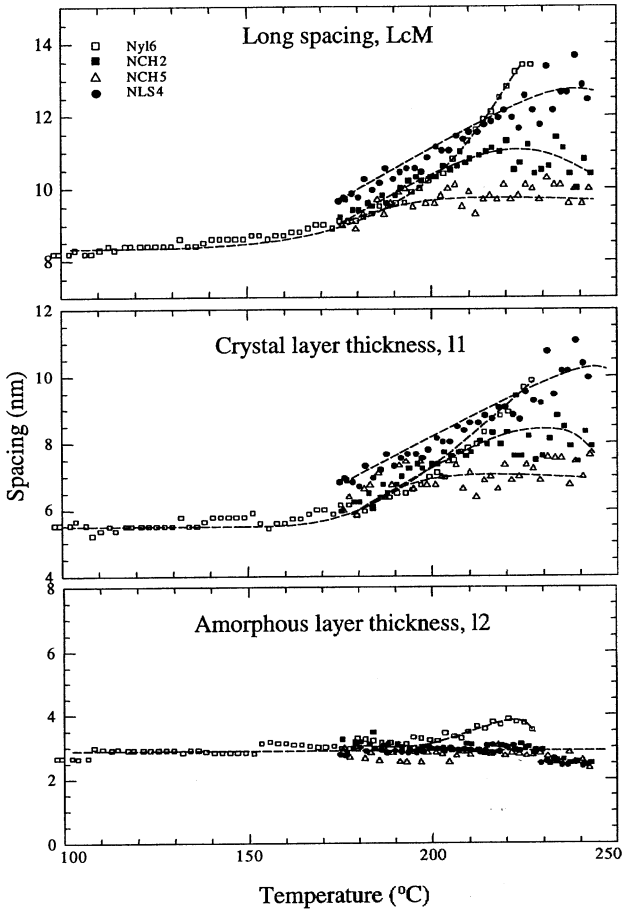


Fig. 10. The long spacing, crystal layer thickness and amorphous layer thickness of the crystal lamellae present in compression molded nylon and the nanocomposites at various temperatures. The lines are drawn as a guide to the eye and are not intended to represent a mathematical fit of the data.

Correlation function analysis of the SAXS data provides details of the lamellar stack structure. Fig. 10 summarizes the long spacing, crystal layer thickness and amorphous layer thickness of the lamellar stacks present in nylon 6 and the nanocomposites. Note that it is not possible to differentiate the types or amount of each crystalline phase ($\alpha$ or $\gamma$) that is incorporated into the crystal layer in the lamellar stack superstructure for this data.

The long spacing of nylon 6 increases with temperature. This consists of a slight coarsening ($\sim$1 nm) of the amorphous layer and approximately 4.5 nm growth of the crystalline layer. Although a fraction of this expansion can be attributed to thermal expansion, the majority of the growths is associated with the melting of thinner crystallites at lower temperatures and the coarsening of larger, thicker crystallites at higher temperatures, resulting in the increase of the mean long-spacing (determined by X-ray diffraction) [32].

In contrast, the long-spacing of the nanocomposites, which is comparable to pure nylon at 175°C, does not increase as rapidly with temperature. The thickness of the amorphous layer is constant and the thickness of the crystalline layer only expands $\sim$1–2.5 nm. Thus, coarsening of the larger crystallites and melting of thinner lamellae is suppressed in the presence of the dispersed silicate layers. Furthermore, strong interfacial interactions further impact the elevated temperature behavior of the lamellar stacks. NCH2 and NCH5 crystal layers ($\sim$8 nm) and long spacings ($\sim$10.5 nm) are generally smaller than the crystal layers ($\sim$10 nm) and long spacings ($\sim$13 nm), of the pure polymer and NLS4.

These observations are consistent with studies based on linear viscoelasticity of NCH5 compressed samples [33] which indicated that the silicate layers are percolated at 5 wt%. If the layers serve as heterogeneous nucleation sites and template crystal growth, the polymer lamellar stacks emerging from the silicate surface will rapidly impinge on neighboring polymer crystallites resulting in a large fraction of smaller less perfected polymer crystallites.

## 4. Conclusions

In summary, semicrystalline PLSN are complex three-phase nanoscale systems. Establishment of structure–property relationships must determine the role of the dispersed silicate layers on the polymer crystal phase, its response to processing environments and the temporal behavior of its morphology at elevated temperatures.

For nylon 6 nanocomposites, the synergism between the layered silicate and the development of the polymer crystalline morphology results in an enhanced stability of the polymer crystalline regions at elevated temperature which depends on silicate loading and polymer–silicate interactions. Additionally, the presence of the layers restricts lamellae coarsening, implying retardation of chain mobility and alteration of the chain conformations. Specifically, for the process history examined, nylon 6 exhibits predominantly $\alpha$-phase behavior from room temperature to melting with a gradual shift in chain–chain and sheet–sheet spacings from $\sim$100°C to melting. In contrast, the presence of aluminosilicate layers stabilizes a dominant $\gamma$-crystal phase, which persists, essentially unmodified, until melting. The temperature dependence of the total crystallinity and the relative fractions of $\alpha$- and $\gamma$-phases is strongly dependent on the layered silicate content and the interaction between the nylon 6 and the aluminosilicate layers. Additionally, the temperature dependence of the of $\alpha$- and $\gamma$-phases imply the $\gamma$-phase is preferentially in proximity of the silicate layers, where as the $\alpha$-phase exists removed from the polymer–silicate interphase region.

Thus, process history and use-temperature will determine the relative fraction of the crystalline polymer phases in semi-crystalline polymer nanocomposites, and thus have significant influence on the elevated temperature properties of such nanocomposites. The percolation of rigid phases, such as the layered silicate and lamellar stacks and

subsequent stability at use-temperatures will determine load transfer and maximum use temperature and elevated temperature mechanical properties. Stabilization of crystalline phases (γ-form) throughout the temperature range may provide an explanation of the higher HDT observed for nylon 6 nanocomposites. Further efforts to deconvolute the contribution of the layered silicate from that of the modified polymer crystalline morphology should utilize different process histories to correlate modifications to the polymer crystalline regions with mechanical response of the semicrystalline PLSN.

## Acknowledgements

Partial funding was provided by the Air Force Office of Scientific Research and the Air Force Research Laboratory, Materials and Manufacturing Directorate. The authors would also like to acknowledge the help of F. Yeh (in situ SAXS and WAXS experiments at Brookhaven National Laboratory); and helpful discussions with D. Hunter. The Advanced Polymers Beamline is supported by DOE (DE-FG02-99ER 45760) and the APPRT.

## References

[1] Kojima Y, Usuki A, Kawasumi M, Okada O, Fukushima Y, Kurachi T, Kamigaito O. J Mater Res 1993;8:1185.
[2] Ke Y, Long C, Qi Z. J Appl Polym Sci 1999;71:1139.
[3] Liu L, Qi Z, Zhu X. J Appl Polym Sci 1999;71:1133.
[4] Messersmith PB, Giannelis EP. J Polym Sci Part A: Polym Chem 1995;33:1047.
[5] Akelah A, Moet A. J Mater Sci 1996;31:3589.
[6] Kojima Y, Usuki A, Kawasumi M, Okada A, Kurachi T, Kamigaito O. J Appl Polym Sci 1993;49:1259.
[7] Yano K, Usuki A, Kurachi T, Kamigaito O. J Polym Sci Part A: Polym Chem 1993;31:2493.
[8] Gilman JW, Kashiwagi T, Lichtenhan JD. SAMPE J 1997;33:40.
[9] Lincoln DM, Vaia RA, Benson Tolle TH, Brown JM. IEEE Aerospace Conference Proceedings, Conference Proceedings of 2000 meeting. IEEE Aerospace Conference on Big Sky, MT March 18–March 25, 2000.
[10] Hseih D-T, Lloyd TB, Rutledge SK. Int SAMPE Symp Proc, Conf Proc 1998 Meet (part 2 of 2) 1998;43(2):1170–1 SAMPE Covina, CA.
[11] Vaia RA, Price G, Ruth PN, Nguyen HT, Lichtenhan J. Appl Clay Sci 1999;15:67.
[12] Alexandre M, Dubois P. Mater Sci Engng 2000;8:1.
[13] Ito M, Mizuochi K, Kanamoto T. Polymer 1998;39:4593.
[14] Lincoln DM, Vaia RA, Wang Z-G, Hsiao BS. Polymer 2000;42:1621.
[15] Usuki A, Kojima Y, Kawasumi M, Okada A, Kukushima Y, Kurauchi T, Kamigaito O. J Mater Res 1993;8:1179.
[16] Krishnamoorti R, Giannelis EP. Macromolecules 1997;30:4097.
[17] Cho JW, Paul DR. Polymer 2001;42:1083.
[18] Inoune M. J Polym Sci A 1963;1:2697.
[19] Hsiao BS, Gardner KH, Wu DQ, Chu B. Polymer 1988;29:1745.
[20] European Molecular Biological Lab., EMBL-Grenoble, Rapp G, Gabriel A, Dosiere M, Kock MHJ. Nucl Instrum Meth Phys Res A 1995;357:178.
[21] Li R, Hu X. Polym Degrad Stab 1998;62:523.
[22] Verdonck E, Schaap K, Thomas LC. Int J Pharm 1999;192:3.
[23] Kojima Y, Matsuoka T, Takahashi H, Kurachi T. J Appl Polym Sci 1994;51:683.
[24] Parker JP, Lindenmeyer PH. J Appl Polym Sci 1977;21:821.
[25] Lincoln DM, Vaia RA, Wang Z-G, Hsiao BS, Krishnamoorti R. Submitted for publication.
[26] Murthy NS, Aharoni SM, Szollosi AB. J Polym Sci: Polym Phys Ed 1985;23:2549.
[27] Murthy NS, Curran SA, Aharoni SM, Minor H. Macromolecules 1991;24:3215.
[28] Vasanthan N, Murthy NS, Bray RG. Macromolecules 1998;31:8433.
[29] Itoh T. Jpn J Appl Phys 1976;15:2295.
[30] Vaia RA, Lincoln D. In: Vaia RA, Krishnamoorti R, editors. Polymer nanocomposites, ACS Symposium Series. Washington, DC: American Chemical Society, 2001.
[31] Verma R, Marand H, Hsiao BS. Macromolecules 1996;29:7767.
[32] Wang W, Schultz JM, Hsiao BS. Macromolecules 1997;30:4544.
[33] Krishnamoorti R, Silva AS. In: Pinnavaia TJ, Beall G, editors. Polymer–clay nanocomposites. New York: Wiley, 2000. p. 315.